DESY 98-044 ISSN 0418-9833

Multiplicity Structure of the Hadronic Final State in Diffractive Deep-Inelastic Scattering at HERA

H1 Collaboration

Abstract

The multiplicity structure of the hadronic system X produced in deep-inelastic processes at HERA of the type $ep \to eXY$, where Y is a hadronic system with mass $M_Y < 1.6$ GeV and where the squared momentum transfer at the pY vertex, t, is limited to $|t| < 1$ GeV^2, is studied as a function of the invariant mass M_X of the system X. Results are presented on multiplicity distributions and multiplicity moments, rapidity spectra and forward-backward correlations in the centre-of-mass system of X. The data are compared to results in e^+e^- annihilation, fixed-target lepton-nucleon collisions, hadro-produced diffractive final states and to non-diffractive hadron-hadron collisions. The comparison suggests a production mechanism of virtual photon dissociation which involves a mixture of partonic states and a significant gluon content. The data are well described by a model, based on a QCD-Regge analysis of the diffractive structure function, which assumes a large hard gluonic component of the colourless exchange at low Q^2. A model with soft colour interactions is also successful.

To be submitted to Eur. Phys. J.

C. Adloff[34], M. Anderson[22], V. Andreev[25], B. Andrieu[28], V. Arkadov[35], I. Ayyaz[29], A. Babaev[24], J. Bähr[35], J. Bán[17], P. Baranov[25], E. Barrelet[29], R. Barschke[11], W. Bartel[11], U. Bassler[29], P. Bate[22], M. Beck[13], A. Beglarian[11,40], H.-J. Behrend[11], C. Beier[15], A. Belousov[25], Ch. Berger[1], G. Bernardi[29], G. Bertrand-Coremans[4], P. Biddulph[22], J.C. Bizot[27], K. Borras[8], V. Boudry[28], A. Braemer[14], W. Braunschweig[1], V. Brisson[27], D.P. Brown[22], W. Brückner[13], P. Bruel[28], D. Bruncko[17], J. Bürger[11], F.W. Büsser[12], A. Buniatian[32], S. Burke[18], G. Buschhorn[26], D. Calvet[23], A.J. Campbell[11], T. Carli[26], E. Chabert[23], M. Charlet[11], D. Clarke[5], B. Clerbaux[4], S. Cocks[19], J.G. Contreras[8], C. Cormack[19], J.A. Coughlan[5], M.-C. Cousinou[23], B.E. Cox[22], G. Cozzika[9], J. Cvach[30], J.B. Dainton[19], W.D. Dau[16], K. Daum[39], M. David[9], A. De Roeck[11], E.A. De Wolf[4], B. Delcourt[27], C. Diaconu[23], M. Dirkmann[8], P. Dixon[20], W. Dlugosz[7], K.T. Donovan[20], J.D. Dowell[3], A. Droutskoi[24], J. Ebert[34], G. Eckerlin[11], D. Eckstein[35], V. Efremenko[24], S. Egli[37], R. Eichler[36], F. Eisele[14], E. Eisenhandler[20], E. Elsen[11], M. Enzenberger[26], M. Erdmann[14], A.B. Fahr[12], L. Favart[4], A. Fedotov[24], R. Felst[11], J. Feltesse[9], J. Ferencei[17], F. Ferrarotto[32], K. Flamm[11], M. Fleischer[8], G. Flügge[2], A. Fomenko[25], J. Formánek[31], J.M. Foster[22], G. Franke[11], E. Gabathuler[19], K. Gabathuler[33], F. Gaede[26], J. Garvey[3], J. Gayler[11], M. Gebauer[35], R. Gerhards[11], S. Ghazaryan[11,40], A. Glazov[35], L. Goerlich[6], N. Gogitidze[25], M. Goldberg[29], I. Gorelov[24], C. Grab[36], H. Grässler[2], T. Greenshaw[19], R.K. Griffiths[20], G. Grindhammer[26], C. Gruber[16], T. Hadig[1], D. Haidt[11], L. Hajduk[6], T. Haller[13], M. Hampel[1], V. Haustein[34], W.J. Haynes[5], B. Heinemann[11], G. Heinzelmann[12], R.C.W. Henderson[18], S. Hengstmann[37], H. Henschel[35], R. Heremans[4], I. Herynek[30], K. Hewitt[3], K.H. Hiller[35], C.D. Hilton[22], J. Hladký[30], D. Hoffmann[11], T. Holtom[19], R. Horisberger[33], V.L. Hudgson[3], M. Ibbotson[22], Ç. İşsever[8], H. Itterbeck[1], M. Jacquet[27], M. Jaffre[27], D.M. Jansen[13], L. Jönsson[21], D.P. Johnson[4], H. Jung[21], M. Kander[11], D. Kant[20], U. Kathage[16], J. Katzy[11], H.H. Kaufmann[35], O. Kaufmann[14], M. Kausch[11], I.R. Kenyon[3], S. Kermiche[23], C. Keuker[1], C. Kiesling[26], M. Klein[35], C. Kleinwort[11], G. Knies[11], J.H. Köhne[26], H. Kolanoski[38], S.D. Kolya[22], V. Korbel[11], P. Kostka[35], S.K. Kotelnikov[25], T. Krämerkämper[8], M.W. Krasny[29], H. Krehbiel[11], D. Krücker[26], A. Küpper[34], H. Küster[21], M. Kuhlen[26], T. Kurča[35], B. Laforge[9], R. Lahmann[11], M.P.J. Landon[20], W. Lange[35], U. Langenegger[36], A. Lebedev[25], M. Lehmann[16], F. Lehner[11], V. Lemaitre[11], S. Levonian[11], M. Lindstroem[21], B. List[11], G. Lobo[27], V. Lubimov[24], D. Lüke[8,11], L. Lytkin[13], N. Magnussen[34], H. Mahlke-Krüger[11], E. Malinovski[25], R. Maraček[17], P. Marage[4], J. Marks[14], R. Marshall[22], G. Martin[12], R. Martin[19], H.-U. Martyn[1], J. Martyniak[6], S.J. Maxfield[19], S.J. McMahon[19], T.R. McMahon[19], A. Mehta[5], K. Meier[15], P. Merkel[11], F. Metlica[13], A. Meyer[12], A. Meyer[11], H. Meyer[34], J. Meyer[11], P.-O. Meyer[2], A. Migliori[28], S. Mikocki[6], D. Milstead[19], J. Moeck[26], R. Mohr[26], S. Mohrdieck[12], F. Moreau[28], J.V. Morris[5], E. Mroczko[6], D. Müller[37], K. Müller[11], P. Murín[17], V. Nagovizin[24], B. Naroska[12], Th. Naumann[35], I. Négri[23], P.R. Newman[3], D. Newton[18], H.K. Nguyen[29], T.C. Nicholls[11], F. Niebergall[12], C. Niebuhr[11], Ch. Niedzballa[1], H. Niggli[36], O. Nix[15], G. Nowak[6], T. Nunnemann[13], H. Oberlack[26], J.E. Olsson[11], D. Ozerov[24], P. Palmen[2], E. Panaro[11], A. Panitch[4], C. Pascaud[27], S. Passaggio[36], G.D. Patel[19], H. Pawletta[2], E. Peppel[35], E. Perez[9], J.P. Phillips[19], A. Pieuchot[11], D. Pitzl[36], R. Pöschl[8], G. Pope[7], B. Povh[13], K. Rabbertz[1], P. Reimer[30], B. Reisert[26], H. Rick[11], S. Riess[12], E. Rizvi[11], P. Robmann[37], R. Roosen[4], K. Rosenbauer[1], A. Rostovtsev[24,11], F. Rouse[7], C. Royon[9], S. Rusakov[25], K. Rybicki[6], D.P.C. Sankey[5], P. Schacht[26], J. Scheins[1], S. Schiek[11], S. Schleif[15], P. Schleper[14], D. Schmidt[34], G. Schmidt[11], L. Schoeffel[9], V. Schröder[11], H.-C. Schultz-Coulon[11], B. Schwab[14], F. Sefkow[37], A. Semenov[24], V. Shekelyan[26], I. Sheviakov[25], L.N. Shtarkov[25], G. Siegmon[16], U. Siewert[16], Y. Sirois[28], I.O. Skillicorn[10], T. Sloan[18], P. Smirnov[25], M. Smith[19], V. Solochenko[24], Y. Soloviev[25], A. Specka[28], J. Spiekermann[8], H. Spitzer[12], F. Squinabol[27], P. Steffen[11], R. Steinberg[2], J. Steinhart[12], B. Stella[32], A. Stellberger[15], J. Stiewe[15], U. Straumann[14], W. Struczinski[2], J.P. Sutton[3], M. Swart[15], S. Tapprogge[15], M. Taševský[31], V. Tchernyshov[24], S. Tchetchelnitski[24], J. Theissen[2], G. Thompson[20], P.D. Thompson[3], N. Tobien[11], R. Todenhagen[13], P. Truöl[37], G. Tsipolitis[36], J. Turnau[6], E. Tzamariudaki[11], S. Udluft[26], A. Usik[25], S. Valkár[31], A. Valkárová[31], C. Vallée[23], P. Van Esch[4], P. Van Mechelen[4], Y. Vazdik[25], G. Villet[9], K. Wacker[8], R. Wallny[14], T. Walter[37], B. Waugh[22], G. Weber[12], M. Weber[15], D. Wegener[8], A. Wegner[26], T. Wengler[14], M. Werner[14], L.R. West[3], S. Wiesand[34], T. Wilksen[11], S. Willard[7], M. Winde[35], G.-G. Winter[11], C. Wittek[12], E. Wittmann[13], M. Wobisch[2],

H. Wollatz[11], E. Wünsch[11], J. Žáček[31], J. Zálešák[31], Z. Zhang[27], A. Zhokin[24], P. Zini[29], F. Zomer[27], J. Zsembery[9] and M. zurNedden[37]

[1] I. Physikalisches Institut der RWTH, Aachen, Germany[a]
[2] III. Physikalisches Institut der RWTH, Aachen, Germany[a]
[3] School of Physics and Space Research, University of Birmingham, Birmingham, UK[b]
[4] Inter-University Institute for High Energies ULB-VUB, Brussels; Universitaire Instelling Antwerpen, Wilrijk; Belgium[c]
[5] Rutherford Appleton Laboratory, Chilton, Didcot, UK[b]
[6] Institute for Nuclear Physics, Cracow, Poland[d]
[7] Physics Department and IIRPA, University of California, Davis, California, USA[e]
[8] Institut für Physik, Universität Dortmund, Dortmund, Germany[a]
[9] DSM/DAPNIA, CEA/Saclay, Gif-sur-Yvette, France
[10] Department of Physics and Astronomy, University of Glasgow, Glasgow, UK[b]
[11] DESY, Hamburg, Germany[a]
[12] II. Institut für Experimentalphysik, Universität Hamburg, Hamburg, Germany[a]
[13] Max-Planck-Institut für Kernphysik, Heidelberg, Germany[a]
[14] Physikalisches Institut, Universität Heidelberg, Heidelberg, Germany[a]
[15] Institut für Hochenergiephysik, Universität Heidelberg, Heidelberg, Germany[a]
[16] Institut für experimentelle und angewandte Physik, Universität Kiel, Kiel, Germany[a]
[17] Institute of Experimental Physics, Slovak Academy of Sciences, Košice, Slovak Republic[f,j]
[18] School of Physics and Chemistry, University of Lancaster, Lancaster, UK[b]
[19] Department of Physics, University of Liverpool, Liverpool, UK[b]
[20] Queen Mary and Westfield College, London, UK[b]
[21] Physics Department, University of Lund, Lund, Sweden[g]
[22] Department of Physics and Astronomy, University of Manchester, Manchester, UK[b]
[23] CPPM, Université d'Aix-Marseille II, IN2P3-CNRS, Marseille, France
[24] Institute for Theoretical and Experimental Physics, Moscow, Russia
[25] Lebedev Physical Institute, Moscow, Russia[f,k]
[26] Max-Planck-Institut für Physik, München, Germany[a]
[27] LAL, Université de Paris-Sud, IN2P3-CNRS, Orsay, France
[28] LPNHE, Ecole Polytechnique, IN2P3-CNRS, Palaiseau, France
[29] LPNHE, Universités Paris VI and VII, IN2P3-CNRS, Paris, France
[30] Institute of Physics, Academy of Sciences of the Czech Republic, Praha, Czech Republic[f,h]
[31] Nuclear Center, Charles University, Praha, Czech Republic[f,h]
[32] INFN Roma 1 and Dipartimento di Fisica, Università Roma 3, Roma, Italy
[33] Paul Scherrer Institut, Villigen, Switzerland
[34] Fachbereich Physik, Bergische Universität Gesamthochschule Wuppertal, Wuppertal, Germany[a]
[35] DESY, Institut für Hochenergiephysik, Zeuthen, Germany[a]
[36] Institut für Teilchenphysik, ETH, Zürich, Switzerland[i]
[37] Physik-Institut der Universität Zürich, Zürich, Switzerland[i]
[38] Institut für Physik, Humboldt-Universität, Berlin, Germany[a]
[39] Rechenzentrum, Bergische Universität Gesamthochschule Wuppertal, Wuppertal, Germany[a]
[40] Vistor from Yerevan Physics Institute, Armenia

[a] Supported by the Bundesministerium für Bildung, Wissenschaft, Forschung und Technologie, FRG, under contract numbers 7AC17P, 7AC47P, 7DO55P, 7HH17I, 7HH27P, 7HD17P, 7HD27P, 7KI17I, 6MP17I and 7WT87P
[b] Supported by the UK Particle Physics and Astronomy Research Council, and formerly by the UK Science and Engineering Research Council
[c] Supported by FNRS-NFWO, IISN-IIKW
[d] Partially supported by the Polish State Committee for Scientific Research, grant no. 115/E-

343/SPUB/P03/002/97 and grant no. 2P03B 055 13
[e] Supported in part by US DOE grant DE F603 91ER40674
[f] Supported by the Deutsche Forschungsgemeinschaft
[g] Supported by the Swedish Natural Science Research Council
[h] Supported by GA ČR grant no. 202/96/0214, GA AV ČR grant no. A1010619 and GA UK grant no. 177
[i] Supported by the Swiss National Science Foundation
[j] Supported by VEGA SR grant no. 2/1325/96
[k] Supported by Russian Foundation for Basic Researches grant no. 96-02-00019

1 Introduction

The observation of "Large Rapidity Gap" (LRG) events [1, 2] in deep-inelastic ep scattering (DIS) at HERA, which are mainly attributed to diffractive photon dissociation [3,4], has led to renewed interest in diffractive phenomena [5] and how they can be understood within quantum chromodynamics (QCD). This paper continues a series of final-state studies by H1 [6–9] and ZEUS [10–12] and presents the first results on the charged particle multiplicity structure in LRG events.

Following conventions adopted in earlier H1 analyses [7, 13], the large rapidity gap events studied here are experimentally defined in terms of the generic process $ep \to eXY$, where the hadronic systems X and Y are separated by the largest rapidity gap in the event; Y is the system closest to the outgoing proton beam [7,13,8]. Events with no activity in a large pseudo-rapidity[1] domain adjacent to the outgoing proton beam are selected. In these events the proton either stays intact (Y = proton), or is excited to a low-mass system. The system Y has longitudinal momentum close to that of the proton beam and small transverse momentum. In such events, the system X, measured in the central part of the detector, can be viewed as mainly resulting from the dissociation of a photon with a virtuality Q^2. The requirement of a large rapidity gap implies that the invariant masses M_X and M_Y of the systems X and Y are small compared to W, the centre-of-mass energy of the $\gamma^* p$ system. In the following, the terms "LRG events" and "diffractive events" will be used synonymously, although, in practice, some contribution from non-diffractive and double-diffractive processes is to be expected, particularly at large M_X.

In diffractive DIS it is useful to view the interaction in a Lorentz frame where the target proton is at rest. For small values of Bjorken-x, x_{Bj}, the virtual photon fluctuates far upstream of the proton target into a quark-antiquark pair which can subsequently evolve into a more complex partonic system ($q\bar{q}, q\bar{q}g, \ldots$) before the actual interaction occurs [14–16]. The virtual photon can thus be described as a superposition of Fock-states with different partonic content [17].

Diffraction in general [18], and dissociation of the photon in particular, arises from the fact that the strength of absorption of the various Fock-states depends on the internal degrees of freedom and quark-gluon composition of the dissociating object [19–21]. Specifically, whereas the total $\gamma^* p$ cross section measures the average absorption strength, the magnitude of the diffractive cross section, on the other hand, is related to its fluctuations [19,20]. The diffractively produced hadronic final states are therefore expected to carry information, not only on the parton composition of the virtual photon wavefunction components and their interaction with the target, but also on their respective contributions to the diffractive cross section.

Virtual photon dissociation can also be approached from a t-channel perspective. In Regge phenomenology, the interaction takes place via a factorisable exchange of the pomeron ($I\!P$) and of reggeons related to mesons. It has been suggested to endow the pomeron (and reggeons) with a partonic sub-structure and to use the concept of parton distributions in the pomeron and in sub-leading reggeons to model diffractive deep-inelastic scattering [22]. In the proton's infinite-momentum frame, the pomeron (or reggeon) has a fraction $x_{I\!P} = (q \cdot (P - P'))/(q \cdot P)$ of the proton's four-momentum P (q and P' being the four-momentum of the exchanged photon and the system Y, respectively), while the fractional momentum of the exchange carried by the struck parton is $\beta = x_{Bj}/x_{I\!P}$. This approach, adopted in [13] assuming the DGLAP evolution equations [23], indicates, as was already conjectured in [24], that the pomeron must have a large hard gluon content at low Q^2 but that a sub-leading meson exchange is also needed at larger values of $x_{I\!P}$ or M_X, if the basic hypothesis of factorisation of each component is to be maintained.

The parton structure of the colourless exchange, as deduced from an analysis of the total diffractive DIS cross section, can be tested in studies of diffractive final states [8,12,9,25]. These confirm the need for a pomeron dominated by hard gluons at a starting scale $Q_0^2 \sim 3$ GeV^2.

[1]H1 uses a laboratory coordinate system with the z-axis aligned with the proton beam direction. Pseudorapidity is defined as $\eta = -\ln(\tan\frac{\theta}{2})$, where θ is the polar angle with respect to the proton direction.

This paper complements previous work and presents an analysis of charged particle multiplicity distributions, multiplicity moments, charged particle density in rapidity space and forward-backward multiplicity correlations measured in the centre-of-mass (CMS) of the system X. The emphasis is placed on a comparison with data from e^+e^- annihilation, fixed-target DIS, hadron diffraction and soft non-diffractive hadron-hadron collisions. Monte Carlo models which represent various theoretical views on diffraction in DIS [26, 27] are also confronted with the data.

2 Experimental procedure

2.1 The experiment

The experiment was carried out with the H1 detector [28] at the HERA storage ring at DESY. The data were collected during the 1994 running period when 27.5 GeV positrons collided with 820 GeV protons, at a centre-of-mass energy of 300 GeV. The following briefly describes the detector components most relevant to this analysis.

The energy of the scattered positron is measured with a backward electromagnetic lead-scintillator calorimeter (BEMC), extending over the polar angular range $151^\circ < \theta < 177^\circ$ with full azimuthal coverage. The BEMC electromagnetic energy resolution is $\sigma_E/E \approx 0.10/\sqrt{E[\mathrm{GeV}]} \oplus 0.42/E[\mathrm{GeV}] \oplus 0.03$, while the BEMC energy scale for positrons is known to an accuracy of 1% [29]. A backward proportional chamber (BPC), situated immediately in front of the BEMC and with an angular acceptance of $155.5^\circ < \theta < 174.5^\circ$, serves to measure the impact point of the scattered positron and to confirm that the particle entering the BEMC is charged. Using information from the BPC, the BEMC and the reconstructed event vertex, the polar angle of the scattered positron can be determined to better than 1 mrad. A scintillator hodoscope behind the BEMC is used to reject beam-induced background based on a time-of-flight measurement.

The hadronic final state is measured by tracking detectors surrounded by calorimeters. The Central Tracker consists of inner and outer cylindrical jet chambers, z-drift chambers and proportional chambers. The jet chambers, mounted concentrically around the beam line, inside a homogeneous magnetic field of 1.15 Tesla, provide both particle charge and momentum measurement from track curvature and cover an acceptance region defined by the angular interval $15^\circ < \theta < 165^\circ$ and transverse momentum $p_T > 0.1$ GeV. Up to 56 space points can be measured for tracks with sufficiently large p_T. The resolutions achieved are $\sigma_{p_T}/p_T \approx 0.009 \cdot p_T\,[\mathrm{GeV}] \oplus 0.015$ and $\sigma_\theta = 20$ mrad [30, 28] with a track finding efficiency above 95% for tracks well contained in both jet chambers. In addition, forward going particles can be detected by the Forward Tracker in the polar angular range $8^\circ < \theta < 20^\circ$. The liquid argon calorimeter (LAr) extends over the polar angular range $4^\circ < \theta < 154^\circ$ with full azimuthal coverage. The LAr hadronic energy resolution is $\sigma_E/E \approx 0.50/\sqrt{E[\mathrm{GeV}]} \oplus 0.02$ as determined in test beams [31]. A study of the transverse momentum balance between the hadronic final state and the scattered positron has shown that the absolute hadronic energy scale is known to an accuracy of 4%. Backward going hadrons can be detected by the BEMC. The hadronic energy scale of the BEMC is known to a precision of 20% [29].

Forward energy at small angles is observed in several detectors near the outgoing proton beam direction. Particles reach these detectors both directly from the interaction point and as a result of secondary scattering with the beam pipe and other adjacent passive material. The detectors are thus sensitive to energetic particles produced in directions that are beyond their geometrical acceptances. The effective ranges of sensitivity to energy flow are $3.5 \lesssim \eta \lesssim 5.5$ for the copper/silicon sandwich (PLUG) calorimeter, $4.5 \lesssim \eta \lesssim 6.5$ for the Forward Muon Spectrometer and $6.0 \lesssim \eta \lesssim 7.5$ for the Proton Remnant Tagger, which consists of scintillation counters and is located 24 m from the interaction point [3]. These detectors overlap considerably in their rapidity coverage, thereby allowing for intercalibration of their efficiencies.

2.2 Monte Carlo simulation of LRG events

Monte Carlo generated LRG events obtained with the RAPGAP 2.02 generator [27] are used to correct the observed distributions for detector acceptance, inefficiencies and smearing effects. This model correctly accounts for many final-state features of LRG events [13, 12, 8, 9], but was not tuned to the multiplicity data presented in this paper. All generated events go through a full simulation of the H1 apparatus and are passed through the same analysis chain as the real data. The detector simulation is based on the GEANT program [32]. The RAPGAP predictions shown in subsequent figures were derived from a model version which incorporates the recent results of the QCD-Regge analysis of the diffractive structure function [13]. Results are also shown from the DIS Monte Carlo event generator LEPTO 6.5 [33] and from the JETSET parton-shower model [34] for simulation of e^+e^- annihilation hadronic final states. Important technical aspects of these models are given in recent H1 publications [13, 8, 9] and are not repeated here.

The RAPGAP generator models LRG events as deep-inelastic scattering of a virtual photon off a pomeron or reggeon coupled to the initial-state proton. The pomeron and reggeon are given a partonic content. The meson structure function is taken to be that of the pion [35].

Different partonic sub-processes are implemented using Born-term and first-order perturbative QCD matrix elements: $eq \rightarrow eq$ scattering, QCD-Compton scattering ($eq \rightarrow eqg$) and boson-gluon fusion (BGF) off a gluon in the colourless exchange ($eg \rightarrow eq\bar{q}$). Their relative contributions are controlled by quark and gluon densities of the exchange as determined in the H1 QCD-Regge analysis [13] of the LRG event cross section using the DGLAP evolution equations. In this model a "pomeron remnant" heads in the direction opposite to the virtual photon, consisting of a quark or a gluon for eq or eg scattering, respectively. The fragmentation of the partonic systems created in the sub-processes $eq \rightarrow eq$, $eq \rightarrow eqg$, is thus expected to be analogous to that in e^+e^- annihilation with centre-of-mass energy $\sqrt{s} = M_X$. However, in BGF the initial partonic system consists of a pomeron remnant (gluon) and a $q\bar{q}$ pair in a colour-octet state. This process has no equivalent in e^+e^- annihilation.

To assess the sensitivity to the quark-gluon content of the pomeron, results are presented for two sets of parton distributions (labelled hereafter "RG F_2^D (fit 3)" and "RG F_2^D (fit 1)"): i) a "hard gluon" distribution ("fit 3" in [13]) whereby gluons carry $\geq 80\%$ of the momentum at the starting scale $Q_0^2 = 3$ GeV^2; ii) a "$q\bar{q}$-only" distribution whereby only quarks are present at Q_0^2 ("fit 1" in [13]). The latter model version is disfavoured in fits to $F_2^{D(3)}$ [13] and by diffractive final-state studies reported in [12, 8, 9][2].

Higher-order effects in the QCD cascade are treated with the parton shower model, as implemented in LEPTO [36]. Hadronisation is carried out with the Lund string fragmentation scheme, as in JETSET 7.4 [34]. QED radiative processes are included via an interface to the program HERACLES [37].

Soft colour interactions form the basis of an alternative model, which is implemented in the LEPTO 6.5 [26] generator. In this scheme [38], LRG events are the result of a normal deep-inelastic scattering on the proton followed by a long-time-scale random colour rearrangement in the soft field of the target. This mechanism leads to a fraction of events with a large rapidity gap of the type studied in this paper.

Studies of diffractively produced meson systems in meson-hadron interactions with masses M_X below 10 GeV have revealed striking similarities with e^+e^- final states at $\sqrt{s} = M_X$ (see e.g. [39]). To analyse virtual photon dissociation along similar lines, the JETSET parton shower model for this process is used (labelled hereafter "JETSET-e^+e^-"). The predictions are calculated for a standard mixture of primary (u, d, s) quark-antiquark pairs only. A primary $c\bar{c}$ component ($e^+e^- \rightarrow c\bar{c}$) has been neglected, motivated by the prediction that, for a quark-dominated pomeron, heavy-quark production is suppressed [40]. It was verified, however, that inclusion of a contribution from primary $c\bar{c}$ pairs has little effect on the multiplicity and would

[2]The predictions from fit 2 in [13] are very similar to those of fit 3 for the observables studied here and not shown.

not alter the conclusions of this analysis. The generated e^+e^- events are rotated such that the z-axis coincides with the initial $q\overline{q}$ axis of the event in the CMS. Rapidity[3] is calculated relative to that direction. The use of JETSET-e^+e^- permits a consistent comparison with the H1 data and avoids difficulties due to the differing experimental treatment of e.g. strange particle production in different e^+e^- experiments.

To study the systematic uncertainties arising from background processes, several other Monte Carlo generators are used.

The DIFFVM generator [41] models the low mass region of diffraction ($M_X < 1.1$ GeV) via production of the vector mesons $\rho(770)$, $\omega(782)$ and $\phi(1020)$. This model further includes a simulation of proton diffractive dissociation.

The PHOJET generator [42] is used to estimate background from photoproduction processes. The model simulates non-diffractive reactions, elastic vector meson production, vector meson production with proton dissociation, single-photon diffractive dissociation and double diffraction and is in broad agreement with experimental results at HERA [43].

2.3 Event and track selection

A neutral current DIS event selection is made [44] by demanding a well-reconstructed scattered positron detected in the BEMC with an energy, E'_e, larger than 10 GeV. A subsample of dominantly diffractive events is then selected by requiring no activity above noise levels in any of the forward detectors or in the most forward part ($\eta > 3.2$) of the LAr Calorimeter.

Further cuts are applied to ensure that a positron is detected and reconstructed with high quality. An event vertex, reconstructed from tracks in the central trackers, within $z = \pm 30$ cm of the mean vertex position, is required to reject beam-induced background. Events with a time-of-flight veto from the scintillator hodoscope are rejected.

The standard deep-inelastic kinematic variables (y_{Bj}, Q^2) are reconstructed with the methods described in [13, 7] and which use both the scattered positron and the hadronic final state. The kinematic variables ($x_{I\!P}$, M_X) characterising the final state in LRG events, are obtained from a combination of tracker and calorimeter information with an algorithm for track-cluster association which avoids double counting. In [13, 7] it is demonstrated that M_X is adequately reconstructed across the kinematic range of the measurement with a resolution of about 25%.

Corrected data are restricted to a kinematic region where the acceptance of the H1 detector is high and the contribution from non-DIS background is low. Together with the requirement $E'_e > 10$ GeV, an upper limit on y_{Bj} at 0.6 ensures that the photoproduction background is less than 0.3% in the selected event sample. The lower limit $y_{Bj} > 0.05$ ensures substantial hadronic energy flow in the detector and adequate resolution in y_{Bj}. The y_{Bj} cuts correspond roughly to a range $70 < W < 230$ GeV. Non-diffractive contributions are suppressed by requiring $x_{I\!P} < 0.05$. A lower cut on M_X of 3 GeV excludes light vector meson contributions. In addition, the requirement of an absence of activity in the forward detectors imposes the approximate restrictions $M_Y \lesssim 1.6$ GeV and $|t| \lesssim 1$ GeV^2, although these variables were not measured directly. The kinematic regions to which the data are corrected are summarised in Table 1; there $|t_{min}|$ is the minimal kinematically allowed value of $|t|$. The event sample consists of 4738 events, corresponding to an integrated luminosity of 1.3 pb^{-1}.

The multiplicity analysis is based on charged particles. Only tracks observed within the acceptance of the central tracking detector, and which are successfully fitted to the primary event vertex, contribute to the uncorrected multiplicity. Further details on the track selection criteria and efficiencies can be found in [44].

The multiplicity distribution is corrected with an iterative matrix migration method based on full Monte Carlo simulation of the detector response. The method is described in detail in [45, 44]. The results are cross-checked with a fit of a Negative Binomial distribution, smeared for

[3]Rapidity of a particle is defined as $y = 0.5 \ln[(E + p_z)/(E - p_z)]$, where E is the energy and p_z the momentum component along the direction of a predefined axis; the pion mass is assigned to each particle.

Quantity	Lower limit	Upper limit
Q^2	7.5 GeV^2	100 GeV^2
y_{Bj}	0.05	0.6
$x_{I\!P}$	0.0003	0.05
M_X	3 GeV	36 GeV
$\|t\|$	$\|t_{min}\|$	1 GeV^2
M_Y	proton mass	1.6 GeV

Table 1: Limits of the kinematic regions considered for corrected data.

detector acceptance and inefficiencies, to the observed multiplicity distribution. This parametric technique is known to be less sensitive to the generator input, but yields only the lowest moments of the multiplicity distribution. For the measurement of rapidity spectra, a standard bin-by-bin correction procedure is used, with cross-checks provided by the matrix-unfolding methods.

Charged decay products of K_S^0, Λ and $\overline{\Lambda}$ and from weakly decaying particles with lifetimes larger than $8 \cdot 10^{-9}$ s are subtracted from the multiplicity distribution through the unfolding method [44]. Hadrons associated with the target remnant system Y are excluded from the multiplicity measurement.

2.4 Systematic errors

Several sources of possible systematic errors are investigated. The analysis is repeated for each source and the changes to the results are added in quadrature. For illustration, the typical systematic error on the mean total charged multiplicity and on the central rapidity ($-0.5 < y < 0.5$) particle density are given in square brackets for each source separately.

- The error due to the uncertainty of the energy scale of the hadronic final state is estimated by scaling the LAr, BEMC and Central Tracker energies by ±4%, ±20% and ±3% respectively [0.4%, 0.4%].

  The systematic uncertainty in the reconstruction of the scattered positron is studied by varying the energy E'_e and polar angle θ' by ±1% and ±1 mrad, respectively [0.3%, 0.9%].

- The influence of the pomeron (reggeon) flux and pomeron (reggeon) structure function used in the Monte Carlo generator for correction is investigated by reweighing the β, $x_{I\!P}$ and t distributions for Monte Carlo events as in [13] [β: 1.3%, 2.2%; $x_{I\!P}$: 0.3%, 1.6%; t: 1.1%, 3.5%].

- Both the colour dipole model, as in ARIADNE [46], and the parton shower model are used to evaluate the influence of these event generation schemes on the corrections. The full difference is taken as the systematic error [0.6%, 0.6%].

- The strangeness-suppression parameter (`PARJ(2)` in JETSET [34]), affecting the rate of strange particle production in the simulation of the fragmentation process, has been varied in the range 0.2–0.3 according to recent results on strange particle production [47,48] [0.1%, 0.1%].

- Track-quality criteria (such as the track length and the number of hits) are varied to estimate systematic errors related to an imperfect description of the acceptance and efficiency of the Central Tracker in the Monte Carlo simulation [1.3%, 3.1%].

  An uncertainty of 30% is assumed on the Monte Carlo correction outside the tracker acceptance (θ_{LAB} outside the range 8°–165° or $p_T^{lab} < 0.1$ GeV; the range between 8°–15° has been cross-checked with data from the Forward Tracker) [3.6%, 1.5%].

- Background events are suppressed by the event selection criteria. Remaining background contamination is estimated by including events simulated with the PHOJET and DIFFVM generators in the Monte Carlo event sample [PHOJET: $< 0.1\%$, $< 0.1\%$; DIFFVM: 0.7%, 1.0%].

  The number of events with initial and final-state QED radiation is changed by $\pm 50\%$ [0.4%, 0.1%].

- A fit to a smeared Negative Binomial distribution is used as a cross-check on the matrix-unfolding results [error on central rapidity particle density 2.8%].

3 Results

All data presented below[4] are corrected for the effects of acceptance and resolution of the H1 detector in the kinematic ranges specified in Table 1. To optimize the statistical precision of the different measurements presented here, a fine- and coarse-grained binning in M_X is used. The requirement of a forward rapidity gap ensures that the hadronic final states of the system X are well contained in the central detectors. The data span the M_X range from 3 to 36 GeV, distributed over the intervals as listed in Table 2. Statistical and systematic errors on the data points shown in the figures are combined in quadrature. Unless otherwise stated, where two error bars are displayed the inner one is the statistical and the outer shows the total error. In comparing H1 LRG data at a given M_X to data from other processes, the corresponding centre-of-mass energy scale is chosen to be W for fixed-target DIS data, $\sqrt{s}$ for e^+e^- and non-diffractive hadron collisions, M_X for hadro-produced diffractive states.

M_X range (GeV)	$\langle M_X \rangle$ (GeV)	$\langle \beta \rangle$	$\langle Q^2 \rangle$ GeV^2	no. of events
3–8	5.4	0.41	21	1492
8–15	11.4	0.17	26	1515
15–30	21.1	0.06	27	1359
4–6	5.0	0.43	22	638
6–8	7.0	0.30	23	530
8–11	9.5	0.21	26	737
11–15	13.0	0.13	26	778
15–19	16.9	0.08	27	543
19–24	21.3	0.06	27	468
24–36	29.1	0.03	27	562

Table 2: Corrected average M_X, β and Q^2 and the number of observed events for the different intervals in M_X considered in this analysis.

3.1 Multiplicity moments

The lowest-order moments of the multiplicity distribution, the average multiplicity $\langle n \rangle$, the dispersion $D = \langle (n - \langle n \rangle)^2 \rangle^{1/2}$ and the normalised second-order factorial moment R_2, have been measured as a function of M_X. The moment R_2 is defined as $R_2 = \tilde{R}_2 / \langle n \rangle^2$ with

$$\tilde{R}_2 = \langle n(n-1) \rangle = \sum_n P_n \, n(n-1). \tag{1}$$

[4] All data are available in numerical form on request and can be retrieved from the Durham HEPDATA database.

The latter quantity is equal to the integral of the inclusive two-particle density over a given domain in phase space and is a measure of the strength of correlations among the produced hadrons [49, 44]. Note that in the case of uncorrelated particle production, the probability to produce n particles, P_n, follows a Poisson distribution with the result that $R_2 \equiv 1$.

Fig. 1a shows the dependence of the mean charged particle multiplicity on M_X in full phase space. The H1 LRG data can be parameterized by a form $\langle n \rangle = a_1 + a_2 \ln M_X^2 + a_3 \ln^2 M_X^2$, with $a_1 = 2.2 \pm 0.4$, $a_2 = 0.08 \pm 0.17$ and $a_3 = 0.21 \pm 0.02$ (χ^2 per degree of freedom = 0.4; statistical errors only), indicating that $\langle n \rangle$ increases faster than the logarithm of the centre-of-mass energy of the system. In non-diffractive DIS at HERA, a similar rate of increase is observed with respect to W [44]. Also shown are measurements of $\langle n \rangle$ for the diffractively produced system X in the reactions $\pi^{\pm} p \to X^{\pm} p$ and $K^+ p \to X^+ p$ [39, 50]. Although the two data sets agree well for $M_X \lesssim 10$ GeV, $\langle n \rangle$ in LRG events exceeds that in meson diffraction at larger masses. There are no meson diffraction results with $M_X \gtrsim 15$ GeV.

The meson-diffraction data are close to the e^+e^- annihilation results, represented here by the predictions from the JETSET parton shower model (dotted line) which is known to reproduce well the e^+e^- multiplicity data over a wide energy range (see e.g. [51, 52]).

Results on the dispersion and the correlation parameter R_2, (Figs. 1b,c) confirm that also the second-order moments in LRG data are similar to meson diffraction and e^+e^- for $M_X \lesssim 10$ GeV within the precision of the measurements[5]. Stronger multiplicity fluctuations and correlations than in e^+e^- are observed at larger M_X. The rise of R_2 with M_X shows that KNO-scaling [53] does not hold in the M_X range studied here.

The similarities seen in Fig. 1a-c have led to the view [54, 39] that in meson diffraction the (mainly longitudinal) momentum exchange with the target leads to an excited meson state which can be pictured as a colour-string of invariant mass M_X stretched between the valence q and $\bar{q}$ of the meson. This string subsequently hadronises in a way similar to a quark pair in $e^+e^- \to q\bar{q}$ at the corresponding centre-of-mass energy $\sqrt{s} = M_X$. A comparative study of the thrust distribution, energy and quantum number flow in the rest-frame of the system X and also in e^+e^- further support this interpretation [55]. For $M_X \lesssim 10$ GeV the same idea has been succesfully applied to proton diffractive dissociation assuming that the baryonic system X now results from the fragmentation of a (valence) quark-diquark string, thus explaining observed similarities with DIS lepton-nucleon data at values of W comparable to M_X [39, 56]. Due to the larger values of Bjorken-x involved, the latter reaction is dominated by quark-diquark fragmentation.

Combining these experimental results, it follows that low-mass diffraction (above the resonance region) in hadron collisions and photon dissociation in DIS at HERA may be interpreted as the hadronisation of a single string, or colour dipole, with colour triplet-antitriplet endpoints. The larger multiplicity moments seen in LRG events for $M_X \gtrsim 10$ GeV relative to the other processes suggest, however, that the above interpretation is incomplete and that high-mass diffraction involves additional mechanisms. Indications from experiment on the possible nature of these mechanisms exist for hadron diffraction.

In high-mass proton diffraction, measurements show that the multiplicity structure of the system X deviates from the expectations for quark-diquark fragmentation and becomes, in fact, similar to that of soft non-diffractive interactions with $\sqrt{s} = M_X$ [57].

Within the framework of the Dual Parton Model (DPM), which is phenomenologically very successful [58], soft non-diffractive collisions are described by the fragmentation of two or more strings corresponding to single or multiple pomeron exchange in the elastic channel. The similarity between non-diffractive and diffractive processes is explained in DPM [59] by assuming that the colourless exchange in the latter becomes resolved in a $q\bar{q}$ pair at large M_X and subsequently interacts with the dissociating hadron. The diffractive state is then described by two

[5]The errors on the NA22 data points for R_2 are derived from published results for $\langle n \rangle$ and $\langle n(n-1) \rangle - \langle n \rangle^2$ whereby the (unknown) correlation between these quantities is neglected. The quoted errors are therefore to be considered as a lower limit on the true error.

colour strings, one stretched between a valence quark of the excited hadron and a quark in the exchange, the other between a diquark and the remaining quark of the $q\bar{q}$ pair.

Multi-string systems are known to lead to a faster than logarithmic increase of $\langle n \rangle$ with energy, to wider multiplicity distributions and stronger long-range particle correlations than single-string fragmentation [58]. It is also important to note that only colour triplet-antitriplet strings are considered in DPM.

Additional mechanisms, besides $q\bar{q}$ fragmentation are included in present models for diffractive DIS. Fig. 1a-c show model calculations with RAPGAP (fit 3) (solid line) which describe the data well. The difference between RAPGAP and JETSET e^+e^- follows from the presence, in RAPGAP, of additional diagrams involving gluons from the colourless exchange, leading to a large contribition from boson-gluon fusion. The partonic state in lowest-order BGF consists of a gluon (the "pomeron remnant") and a $q\bar{q}$ pair in a colour-octet state. The fragmentation of this state allows for various string topologies, including two-string configurations, thus leading one to expect further similarities with large M_X hadron dissociation.

The admixture of the BGF sub-process with the $q\bar{q}$ and QCD-Compton processes naturally explains larger mean multiplicity and stronger fluctuations. On the other hand, the results for RAPGAP (fit 1), with a quark-dominated pomeron leading dominantly to $q\bar{q}$ parton states, are very similar to those of JETSET e^+e^-, as expected, and are not shown.

The data can also be qualitatively understood in the photon dissociation picture of diffraction. The lowest-order ("aligned jet" [15]) excitation ($\gamma^* \to q\bar{q}$) is dominant for $M_X^2 < Q^2$ and leads to a final state similar to that in e^+e^- annihilation. In addition, higher-order fluctuations (such as $\gamma^* \to q\bar{q}g$ where the gluon has low momentum), which resemble the BGF sub-process, are believed to contribute at larger M_X and to effectively interact as an octet-octet colour dipole [16, 60]. Due to the octet colour charge at the dipole end-points, such a system hadronises with a larger mean multiplicity than a $q\bar{q}$ state [61].

The LEPTO model with "soft colour interactions" (dashed curve) is seen to also agree with the H1 data although it predicts somewhat larger multiplicity fluctuations above $M_X \sim 20$ GeV. This model too contains a sizeable BGF contribution. However, diffraction is viewed here as a final-state interaction and does not invoke the notion of colour-neutral exchange.

The moments of the multiplicity distribution for particles with positive and negative rapidity ("forward" and "backward", respectively) are displayed in Figs. 1d-f. Rapidity is calculated in the rest-frame of the system X (the "$\gamma^* I\!\!P$" centre-of-mass system) with the positive longitudinal momentum axis pointing in the γ^* direction[6], assigning the pion mass to each charged track.

The H1 data show no evidence for an asymmetry between forward and backward hemispheres, in contrast to what is observed for the mean multiplicity measured in fixed-target μp DIS ($Q^2 > 4\,\mathrm{GeV}^2$) [62], where the influence of proton fragmentation on the backward-hemisphere multiplicity distribution is known to be substantial.

The μp data in the current fragmentation region, where the comparison with LRG data is most relevant, agree well with the predictions for e^+e^-, as expected for production dominated by quark jets. The LRG results are also here characterized by larger $\langle n \rangle$ and stronger fluctuations above $M_X \gtrsim 10$ GeV.

The RAPGAP and LEPTO models also predict forward-backward symmetry of the single-hemisphere moments and describe the data adequately. The earlier noted differences with e^+e^- annihilation for the full phase space moments are also seen here.

The role of gluons in high-mass photon dissociation is prominent in all the DIS models considered, in contrast to models for hadronic soft diffraction where quark (diquark) fragmentation is dominant. The indication from the models that the pomeron-remnant has a large gluon content also opens interesting opportunities for comparison with gluon-jet fragmentation in other processes.

[6]The pomeron direction cannot be unambiguously determined since the outgoing system Y is not measured. Since its transverse momentum is small, it has been assumed that the $I\!\!P$ direction is collinear with the incident proton in the rest frame of the system X.

3.2 Multiplicity distributions

The multiplicity distributions in full phase space have been measured, separately for negatively and positively charged tracks, in three intervals of M_X. The results are displayed in Fig. 2a-c in the form of a KNO-distribution [53]: $\psi(z) = \langle n \rangle P_n$ plotted as a function of the normalised multiplicity $z = n/\langle n \rangle$. No significant difference is observed between the distributions for positively and negatively charged hadrons. The data are well reproduced by the RAPGAP model (solid curves) although there are indications that it underestimates the high-multiplicity tail of the distribution at large M_X. The comparison with JETSET e^+e^- predictions (at $\sqrt{s} = \langle M_X \rangle$) shows that the multiplicity distribution is broader in the LRG data, indicative of stronger correlations among the hadrons. The predictions for LEPTO are similar to those of RAPGAP.

Figs. 2d-f further illustrate the forward-backward symmetry of the system X, now for the all-charged multiplicity distribution. The RAPGAP and LEPTO predictions are also forward-backward symmetric but tend to fall below the data at large z. The single-hemisphere distributions are closer to the e^+e^- expectations than in full phase space (cfr. Figs. 2a-c). This difference can be understood as the effect of correlations between hadrons emitted in opposite hemispheres which, as will be shown below, are larger in the DIS LRG data.

3.3 Rapidity spectra

The charged particle rapidity density in three intervals of M_X is shown in Fig. 3. The spectrum rises slowly with M_X in the central region and a rapidity plateau develops with increasing phase space. These features confirm earlier observations in hadron diffraction [63, 57, 55] that the diffractive system hadronises in a jet-like manner both in the forward and backward regions [8, 12, 9]. There is no evidence for a significant forward-backward asymmetry of the y-spectra[7] contrary to what is observed in μN interactions [64, 65].

The particle density in the central region is much larger in LRG events than in μN interactions for W values close to $\langle M_X \rangle$. It is also larger than in e^+e^- annihilation (at $\sqrt{s} = \langle M_X \rangle$) according to the JETSET expectation. The RAPGAP (fit 1) model curve is close to JETSET and the fixed-target data and predicts a particle density which is too low. Both RAPGAP with a hard gluon distribution and LEPTO describe the rapidity spectra, although there are small deviations in the lowest M_X bin.

Fig. 4a further compares the M_X dependence of the central particle density (defined as the mean multiplicity in the region $-0.5 < y < 0.5$) in LRG events to e^+e^- expectations, to that in μN collisions [64,65], non-diffractive meson-proton [66] collisions and proton diffraction [67] . The particle density near $y = 0$ is seen to be larger in LRG events than in all the other processes.

The excess particle production relative to that in e^+e^- and μN indicates that additional mechanisms besides hard and soft gluon bremsstrahlung from quarks are needed (cfr. Sect. 3.1).

The comparison with non-diffractive meson-proton and high-mass proton diffraction further shows that the central particle density in processes which are believed [58] to involve two or more strings with colour triplet-antitriplet end-points ($q\bar{q}$ and quark-diquark strings) is also significantly lower than in the LRG data. This, together with previous observations, argues in favour of models which attribute a higher gluonic content to the partonic system created in virtual photon dissociation than in the other processes.

An estimate of the importance of an additional gluonic component may be obtained by assuming that the particle density in the central region is a linear superposition of two contributions, one arising from $q\bar{q}$ fragmentation (including additional QCD radiation), the second from a colour octet-octet string configuration. This hypothesis is in line with expectations from the photon dissociation picture of diffractive DIS (see e.g. [60]).

[7]The rapidity spectra have also been recomputed with rapidity defined along the thrust axis in the CMS of the system X (not shown). Except for the lowest M_X interval, no significant difference is seen with the results in Fig. 3. This is consistent with the observation in [8] that the thrust axis in LRG events is strongly aligned with the γ^* direction in the $\gamma^* I\!P$ system.

Using the EMC data for the former, and JETSET simulations of a colour-singlet gluon-gluon string for the latter, it is found that, at $\langle M_X \rangle = 11.4$ GeV, approximately equal contributions of the two components are needed to explain the particle density at mid-rapidity[8].

The RAPGAP (fit 3) predictions for the central particle density are shown in Fig. 4a. They are compatible with the LRG data only above $M_X \geq 10$ GeV and are nearly M_X independent. The LEPTO model, on the other hand, predicts a rather stronger dependence on M_X, closer to the tendency observed in the H1 data. The enhanced particle density, both in RAPGAP (fit 3) and in LEPTO, are related to the large contribution from boson-gluon fusion. The RAPGAP (fit 1) model version follows closely the JETSET e^+e^- prediction.

In order to investigate the sensitivity of the results to possible contributions from non-diffractive processes, the analysis has been repeated changing the cut $x_{I\!P} < 0.05$ to $x_{I\!P} < 0.025$. Within errors, no significant effect on the results was observed.

3.4 Forward-Backward Correlations

In this section, differences between LRG events and final states in other processes are further examined through a measurement of the correlation between hadrons emitted in opposite event hemispheres. These so-called "forward-backward" correlations are known to be sensitive to finer details of the fragmentation process and, in particular, to the presence in an inclusive event sample of several distinct sub-classes of events [68].

In previous experiments, the forward-backward correlation was analysed by studying the regression between the forward multiplicity, n_F, and the backward multiplicity, n_B. The correlation is usually well parameterised by a simple linear dependence

$$\langle n_F \rangle = a + b \cdot n_B. \tag{2}$$

Forward-backward correlations have not previously been measured in diffractively produced final states. For reasons of statistics, matrix techniques as used in other analyses [69, 51, 52] to unfold the two-dimensional forward and backward multiplicity distributions have not been employed. Instead, the forward-backward correlation parameter is estimated from the separately unfolded and corrected multiplicity distributions in full phase space, in the forward and in the backward hemispheres. Exploiting the relation between the dispersion for the full phase space (D) and that for the forward and backward hemispheres (D_F and D_B), one can define the correlation parameter ρ as

$$\rho = \frac{D^2 - D_F^2 - D_B^2}{2 D_F D_B}. \tag{3}$$

The parameter ρ is identical to the slope b in eqn. (2) in the case of forward-backward symmetric systems [70].

Fig. 4b shows the parameter ρ in three intervals of M_X for the LRG data. Also shown are data on the parameter b for μp collisions [62], for non-diffractive $\pi^\pm/K^\pm p$ collisions compiled in [70] and JETSET predictions for e^+e^-.

In spite of the large errors, there is clear evidence for stronger correlation in LRG events than observed in e^+e^- annihilation [69] and in the μp data for energies above $\gtrsim 10$ GeV. At lower energy, phase space effects are important and mask possible differences in dynamics. The correlation strength in diffractive DIS is comparable to that in meson-proton interactions.

At LEP, where a value of $b \sim 0.1$ is measured, OPAL finds that the small correlation observed in an inclusive sample of e^+e^- events is primarily due to the superposition of events with distinct numbers of jets and, therefore, different average charged multiplicity. Sub-classes of n-jet events ($n \geq 2$) show no or even negative correlations [52,51]. In νp and $\bar{\nu} p$ reactions [71]

[8]This is consistent with the contribution of about 50% from boson-gluon fusion events to the total diffractive cross section estimated with the RAPGAP model; the latter value depends, however, on the $\hat{p_t}^2$ cut-off value, here chosen to be 2 GeV^2 [8].

no clear evidence for correlations is observed. These data therefore show that forward-backward correlations are small at energies where the production mechanism is believed to be dominated by single-string $q\bar{q}$ or quark-diquark fragmentation.

In contrast, abundant data from hadron interactions, compiled in [70], which cover the range $10 \leq \sqrt{s} \leq 900$ GeV, show that the correlation increases logarithmically with energy, with b as large as 0.65 ± 0.01 at $\sqrt{s} = 900$ GeV. The strength and energy dependence of the effect is attributed to strong event-to-event fluctuations of the particle density as occur e.g. in the multi-string Dual-Parton model due to fluctuations in the number of strings and strings overlapping in phase space [68].

The observation of forward-backward correlations in LRG events with a strength comparable to that in soft hadron interactions adds further support to the view that the inclusive sample of DIS LRG events is a mixture of states with distinct hadronisation properties. To disentangle their precise nature and relative contribution, more differential studies will be needed, however.

In present models for diffractive DIS, distinct production processes are readily identified and related, either to the differences in parton composition and absorption probability of virtual photon Fock-states, or to hard quark- and gluon-initiated interactions off a colourless exchange. That a mixture of such contributions leads to significant forward-backward correlations is demonstrated by the predictions for the parameter ρ from RAPGAP-F_2^D (fit 3) (solid line) and LEPTO (dashed) which are close to the H1 data for $M_X \gtrsim 10$ GeV. The large difference between these DIS models and JETSET for e^+e^- illustrates the sensitivity of this correlation measure to differences in the dynamics of these two processes.

4 Summary and conclusions

The charged-particle multiplicity structure of large-rapidity-gap events of the type $\gamma^* p \to XY$ in deep-inelastic scattering at HERA has been measured. The major fraction of these events is generally interpreted as due to diffractive dissociation of the virtual photon on the proton, $\gamma^* p \to Xp$.

Multiplicity distributions, lower-order moments, rapidity spectra and correlations between hadrons emitted in opposite hemispheres in the rest-frame of the system X have been presented as a function of the invariant mass M_X.

The data have been compared with e^+e^- annihilation (at $\sqrt{s} = M_X$), lepton-nucleon data in a W range comparable to the M_X-range in the H1 data, with hadro-produced diffractive final states, and also with data from non-diffractive hadron-hadron collisions at $\sqrt{s} \sim M_X$. The main observations are the following.

- The mean total charged particle multiplicity $\langle n \rangle$ is a function of M_X and increases proportionally to $\ln^2 M_X$. The inclusive rapidity spectrum is forward-backward symmetric in the rest-frame of X. A plateau develops with increasing M_X. Both $\langle n \rangle$ (for $M_X \gtrsim 10$ GeV) and the particle density near $y = 0$ are larger than in DIS at comparable values of W, than in e^+e^- annihilation at $\sqrt{s} = M_X$ and than in hadro-produced diffractive final states. Furthermore, the particle density in this central region is also higher than in non-diffractive collisions at $\sqrt{s} = M_X$.

- For $M_X \gtrsim 10$ GeV, multiplicity fluctuations are larger than in e^+e^- annihilation and than in the current fragmentation region of lepton-nucleon interactions at comparable values of $\sqrt{s}$ and W, respectively. The forward-backward multiplicity correlations are also larger and of comparable strength to those measured in hadron interactions at $\sqrt{s} = M_X$.

The distinctive characteristics of large-rapidity-gap events mentioned can be globally understood if it is assumed that the photon dissociation mechanism involves a mixture of different partonic states wherein gluons play an increasingly important role as M_X increases. A large contribution from gluon-rich states is also required to explain the steep rise with increasing $1/x_{Bj}$, at fixed Q^2, of the diffractive as well as the total virtual-photon proton cross section [72, 16].

Good agreement with the data is achieved with a model which assumes that the diffractive process is initiated by the interaction of a point-like virtual photon with a gluon-dominated colour-singlet object emitted from the proton, as is suggested by a perturbative QCD-Regge analysis based on DGLAP evolution of the diffractive structure function. However, some deviations are seen in the large-n tail of the multiplicity distribution at high M_X.

A model with soft colour interactions which rearrange the colour topology after a normal deep-inelastic scattering also describes the data although the multiplicity fluctuations are somewhat overestimated for M_X larger than about 20 GeV.

The present analysis adds new support for the conclusion, derived from studies of event shapes [12, 8] and from a study of energy flow and single particle momentum spectra [9] in large-rapidity-gap events in H1, that gluons play a prominent role in deep-inelastic diffraction.

Acknowledgements

We are grateful to the HERA machine group whose outstanding efforts made this experiment possible. We thank the engineers and technicians for their work in constructing and now maintaining the H1 detector, our funding agencies for financial support, the DESY technical staff for continual assistance, and the DESY directorate for the hospitality they extend to the non-DESY members of the collaboration.

References

[1] ZEUS Collaboration, M. Derrick *et al.*, Phys. Lett. **B315** (1993) 481.

[2] H1 Collaboration, T. Ahmed *et al.*, Nucl. Phys. **B429** (1994) 477.

[3] H1 Collaboration, T. Ahmed *et al.*, Phys. Lett. **B348** (1995) 681.

[4] ZEUS Collab., M. Derrick *et al.*, Z. Phys. **C68** (1995) 569.

[5] For reviews see: A. Kaidalov, Phys. Rep. **50** (1979) 157; G. Alberi and G. Goggi, Phys. Rep. **74** (1981) 1; K. Goulianos, Phys. Rep. **101** (1983) 169; N. Zotov and V. Tsarev, Sov. Phys. Usp. **31** (1988) 119.

[6] H1 Collaboration, S. Aid *et al.*, Z. Phys. **C70** (1996) 609.

[7] H1 Collaboration, C. Adloff *et al.*, Z. Phys. **C74** (1997) 221.

[8] H1 Collaboration, C. Adloff *et al.*, Eur. Phys. J. **C1** (1998) 495.

[9] H1 Collaboration, C. Adloff *et al.*, *Hadron Production in Diffractive Deep-Inelastic Scattering*, subm. to Phys. Lett. B.

[10] ZEUS Collaboration, M. Derrick *et al.*, Z. Phys. **C67** (1995) 227.

[11] ZEUS Collaboration, J. Breitweg *et al.*, Z. Phys. **C75** (1997) 421.

[12] ZEUS Collaboration, J. Breitweg *et al.*, *Event Shape Analysis of Deep Inelastic Scattering Events with a Large Rapidity Gap at HERA*, DESY 97-202, subm. to Phys. Lett. B.

[13] H1 Collaboration, C. Adloff *et al.*, Z. Phys. **C76** (1997) 613.

[14] B. L. Ioffe, Phys. Lett. **B30** (1969) 123.

[15] J.D. Bjorken, AIP Conference Proceedings No. 6, Particles and Fields Subseries No. 2, Ed. M. Bander, G. Shaw and D. Wong (AIP, New York, 1972); J.D. Bjorken and J. Kogut, Phys. Rev. **D8** (1973) 1341 (1996), `hep-ph/9601363`.

[16] N. N. Nikolaev and B. G. Zakharov, Z. Phys. **C49** (1991) 607, Z. Phys. **C64** (1994) 631.

[17] H. Abramowicz, L. Frankfurt and M. Strikman, Surveys in High Energy Physics **11** (1997) 51.

[18] I. Pomerančuk and E. Feinberg, Dokl. Acad. Nauk, SSSR **93** (1953) 439, E. Feinberg and I. Pomerančuk, Suppl. Nuovo Cimento **3** (1956) 652; M. Good and W. Walker, Phys. Rev. **120** (1960) 1857.

[19] H. Miettinen and J. Pumplin, Phys. Rev. **D18** (1978) 1696.

[20] B. Blättel *et al.*, Phys. Rev. **D47** (1993) 2761.

[21] G. Bertsch, S. J. Brodsky, A. S. Goldhaber and J. G. Gunion, Phys. Rev. Lett. **47** (1981) 297.

[22] G. Ingelman and P. Schlein, Phys. Lett. **B152** (1985) 256; A. Fritzsch and K.H. Streng, Phys. Lett. **B164** (1985) 395; A. Donnachie and P. V. Landshoff, Phys. Lett. **B191** (1987) 309, Nucl. Phys. **B303** (1988) 634; K. Golec–Biernat and J. Kwiecinski, Phys. Lett. **B353** (1995) 329, `hep-ph/9504230`; E. L. Berger, J. C. Collins, D. E. Soper and G. Sterman, Nucl. Phys. **286** (1987) 704.

[23] Yu.L. Dokshitzer, Sov. Phys. JETP 46 (1977) 641; V.N. Gribov and L.N. Lipatov, Sov. J. Nucl. Phys. 15 (1972) 438, 675; L.N. Lipatov, Sov. J. Nucl. Phys. 20 (1975) 95; G. Altarelli and G. Parisi, Nucl. Phys. **B126** (1977) 298.

[24] F. E. Low, Phys. Rev. **D12** (1975) 163; S. Nussinov, Phys. Rev. Lett. **34** (1975) 1286, Phys. Rev. **D14** (1976) 246.

[25] P. Marage, *Diffractive Jet Production*, DIS97, Workshop on Deep-Inelastic Scattering and QCD, Chicago USA, April 1997.

[26] G. Ingelman, A. Edin, and J. Rathsman, "LEPTO 6.5 - A Monte Carlo Generator for Deep Inelastic Lepton-Nucleon Scattering", DESY 96-057.

[27] H. Jung, Comp. Phys. Comm. **86** (1995) 147.

[28] H1 Collaboration, I. Abt *et al.*, Nucl. Instr. and Meth. **A386** (1997) 310 and Nucl. Instr. and Meth. **A386** (1997) 348.

[29] H1 BEMC Group, J. Ban *et al.*, Nucl. Instr. and Meth. **A372** (1996) 399.

[30] H1 Collaboration, C. Adloff *et al.*, Nucl. Phys. **B485** (1997) 3.

[31] H1 Calorimeter Group, B. Andrieu *et al.*, Nucl. Instr. and Meth. **A336** (1993) 460.

[32] R. Brun *et al.*, GEANT3, CERN DD/EE/84-1 (1987).

[33] G. Ingelman, A. Edin and J. Rathsman, Comp. Phys. Comm. **101** (1997) 108.

[34] T. Sjöstrand, Comp. Phys. Comm. **82** (1994) 74.

[35] J.F. Owens, Phys. Rev. **D30** (1984) 943.

[36] G. Ingelman, Proceedings of the 1991 Workshop on Physics at HERA, DESY, Vol. 3 (1992) 1366.

[37] A. Kwiatkowski, H. Spiesberger and H.-J. Möhring, Comp. Phys. Comm. **69** (1992) 155.

[38] A. Edin, G. Ingelman, and J. Rathsman, Phys. Lett. **B366** (1996) 371.

[39] NA22 Collaboration, M. Begalli *et al.*, Z. Phys. **C55** (1992) 531.

[40] S. Brodsky, P. Hoyer and L. Magnea, Phys. Rev. **D55** (1977) 5585.

[41] B. List, *Diffraktive J/ψ-Produktion in Elektron-Proton-Stößen am Speicherring HERA*, Diploma Thesis, Tech. Univ. Berlin, 1993 (unpublished).

[42] R. Engel, Z. Phys. **C66** (1995) 203,
R. Engel and J. Ranft, Phys. Rev. **D54** (1996) 4244.

[43] H1 Collaboration, S. Aid *et al.*, Z. Phys. **C69** (1995) 27.

[44] H1 Collaboration, S. Aid *et al.*, Z. Phys. **C72** (1996) 573.

[45] P. Van Mechelen, *Multiplicity structure of the hadronic final state in deep-inelastic ep scattering*, Ph. D. Thesis, Univ. of Antwerpen, 1998 (unpublished).

[46] L. Lönnblad, Comp. Phys. Comm. **71** (1992) 15.

[47] DELPHI Collaboration, P. Abreu *et al.*, Phys. Lett. **B275** (1992) 231.

[48] E665 Collaboration, M. R. Adams *et al.*, Z. Phys. **C61** (1994) 539.

[49] E.A. De Wolf, I.M. Dremin and W. Kittel, Phys. Rep. **270** (1996) 1.

[50] F.C. Winkelmann *et al.*, Phys. Rev. Lett. **32** (1974) 121; R.L. Cool *et al.*, Phys. Rev. Lett. **48** (1982) 1451.

[51] DELPHI Collaboration, P. Abreu *et al.*, Z. Phys. **C50** (1991) 185; *ibid.* C52 (1991) 271; *ibid.* C56 (1992) 62.

[52] OPAL Collaboration, R. Akers *et al.*, Phys. Lett. **B320** (1994) 417.

[53] Z. Koba, H. B. Nielsen and P. Olesen, Nucl. Phys. **B40** (1972) 317.

[54] S.P. Misra, A.R. Panda and B.K. Parida, Phys. Rev. Lett. **45** (1980) 322.

[55] NA22 Collaboration, M. Adamus *et al.*, Z. Phys. **C39** (1988) 301.

[56] (pp): F.T. Dao *et al.*, Phys. Lett. **45B** (1973) 399; S.J. Barish *et al.*, Phys. Rev. Lett. **31** (1973) 1080; J.W. Chapman *et al.*, Phys. Rev. Lett. **32** (1974) 257; M.G. Albrow *et al.*, Nucl. Phys. **B102** (1976) 275; ($p\bar{p}$) F. Grard *et al.*, Phys. Lett. **59B** (1975) 409; C.P. Ward *et al.*, Nucl. Phys. **B153** (1979) 299.

[57] UA4 Collaboration, D. Bernard *et al.*, Phys. Lett. **B166** (1986) 459.

[58] A. Capella, U.P. Sukhatme, C.-I. Tan and J. Tran Thanh Van, Phys. Lett. **81B** (1979) 68; Phys. Rep. **236** (1994) 225.

[59] V.V. Innocente *et al.* Phys. Lett. **B169** (1986) 285; J. Ranft, Z. Phys. **C33** (1987) 517; S. Roesler, R. Engel and J. Ranft, Z. Phys. **C59** (1993) 481.

[60] M. Wüsthoff, Phys. Rev. **D56** (1997) 4311.

[61] OPAL Collaboration, K. Ackerstaff *et al.*, preprint CERN-PPE-97-105 (1997).

[62] EMC Collaboration, M. Arneodo *et al.*, Nucl. Phys. **B258** (1985) 249.

[63] UA5 Collaboration, R.E. Ansorge *et al.*, Z. Phys. **C33** (1986) 175.

[64] EMC Collaboration, M. Arneodo *et al.*, Z. Phys. **C35** (1987) 417.

[65] E665 Collaboration, M. R. Adams *et al.*, Z. Phys. **C61** (1994) 179.

[66] NA22 Collaboration, M. Adamus *et al.*, Z. Phys. **C37** (1988) 215.

[67] UA4 Collaboration, D. Bernard *et al.*, Phys. Lett. **B186** (1987) 227.

[68] A. Capella and J. Tran Thanh Van, Z. Phys. **C18** (1983) 85; A. Capella and A. Krzywicki, Phys. Rev. **D18** (1978) 4120.

[69] TASSO Collaboration, W. Braunschweig *et al.*, Z. Phys. **C45** (1989) 193.

[70] NA22 Collaboration, V. V. Aivazyan *et al.*, Z. Phys. **C42** (1989) 533.

[71] H. Grässler *et al.*, Nucl. Phys. **B223** (1983) 269.

[72] W. Buchmüller and A. Hebecker, Phys. Lett. **B355** (1995) 573; A. Edin, G. Ingelman and J. Rathsman, Phys. Lett. **B366** (1996) 371; W. Buchmüller, M.F. McDermott and A. Hebecker, Nucl. Phys. **B487** (1997) 283; Erratum-ibid. **B500** (1997) 621.

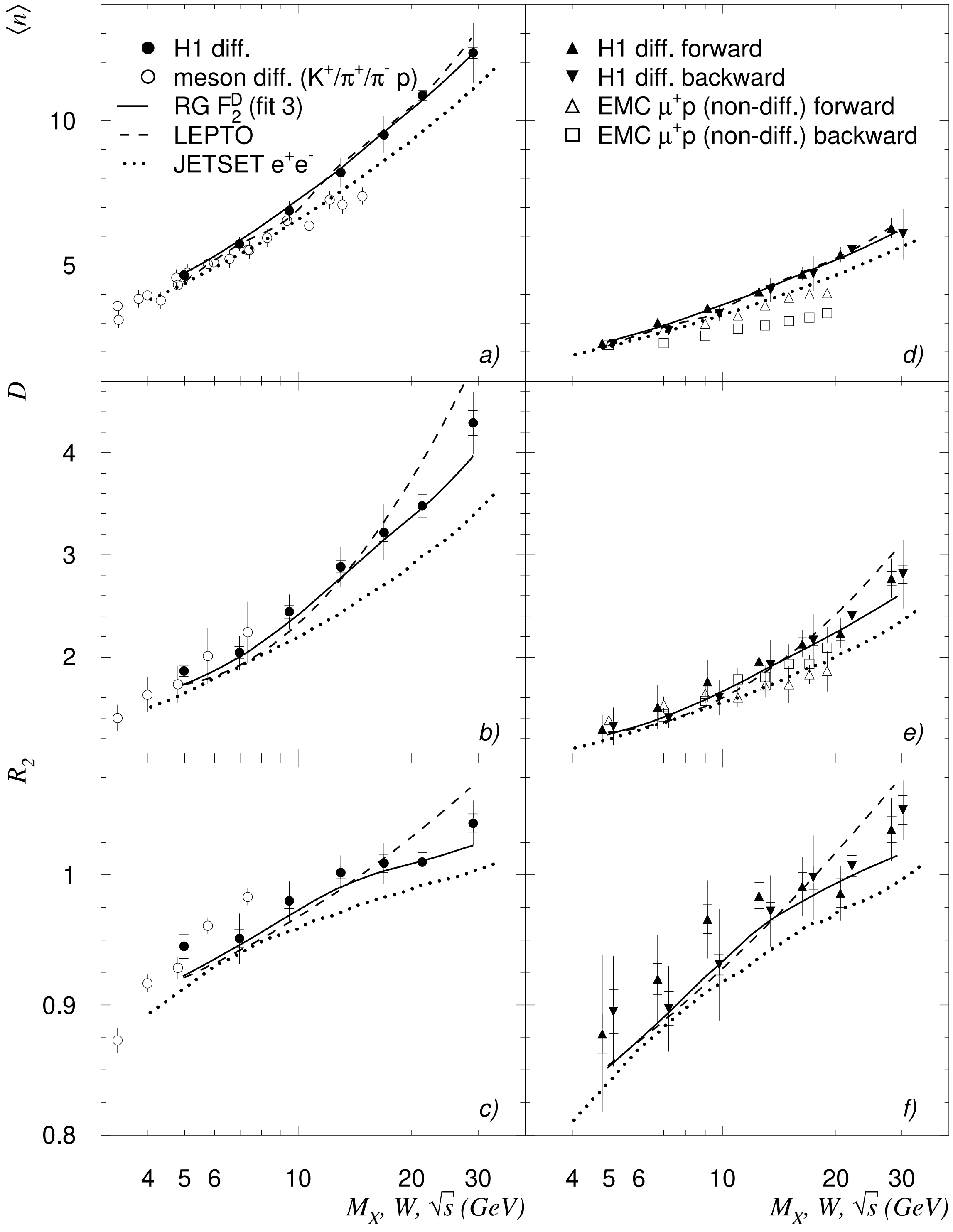

Figure 1: Multiplicity moments $\langle n \rangle$, D and R_2 in full phase space **(a-c)** and in single hemispheres **(d-f)** for charged hadrons as a function of M_X (H1), M_X (meson diffraction), W (EMC), $\sqrt{s}$ (e^+e^-), respectively. For clarity, H1 data points in single hemispheres are slightly shifted in the horizontal direction with respect to their true positions. Also shown are predictions of several Monte Carlo models (see text). The Monte Carlo curves in forward and backward hemispheres are symmetric and their average is plotted.

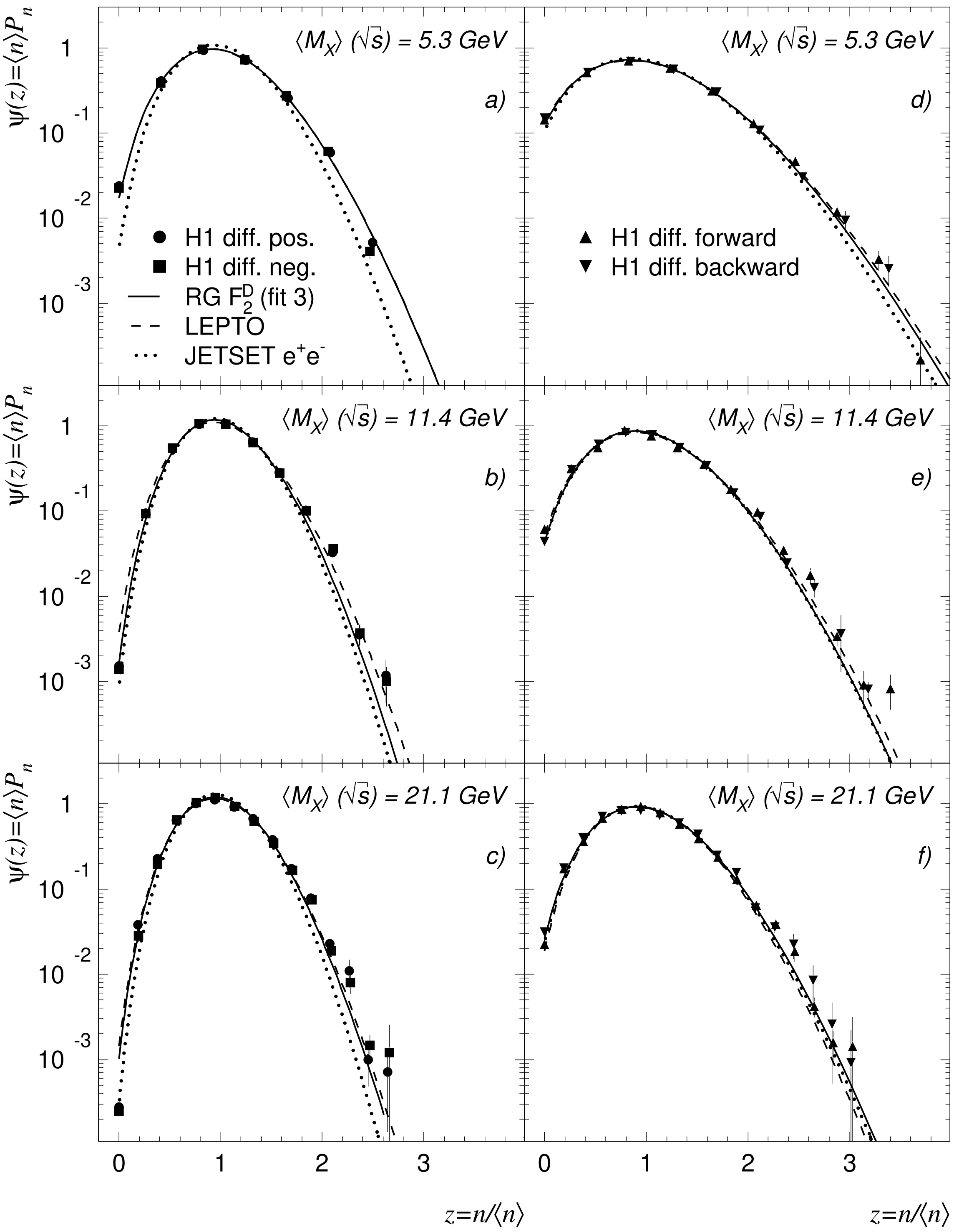

Figure 2: The multiplicity distribution in KNO form for three intervals in M_X (DIS data and Monte Carlo) and at $\sqrt{s} = \langle M_X \rangle$ (JETSET e^+e^-), in full phase space for positive and negative particles separately **(a-c)**, and for all charges in single hemispheres **(d-f)**. The error bars show statistical errors only. Also shown are predictions of several Monte Carlo models (see text). The Monte Carlo curves are charge and forward-backward symmetric and their average is plotted.

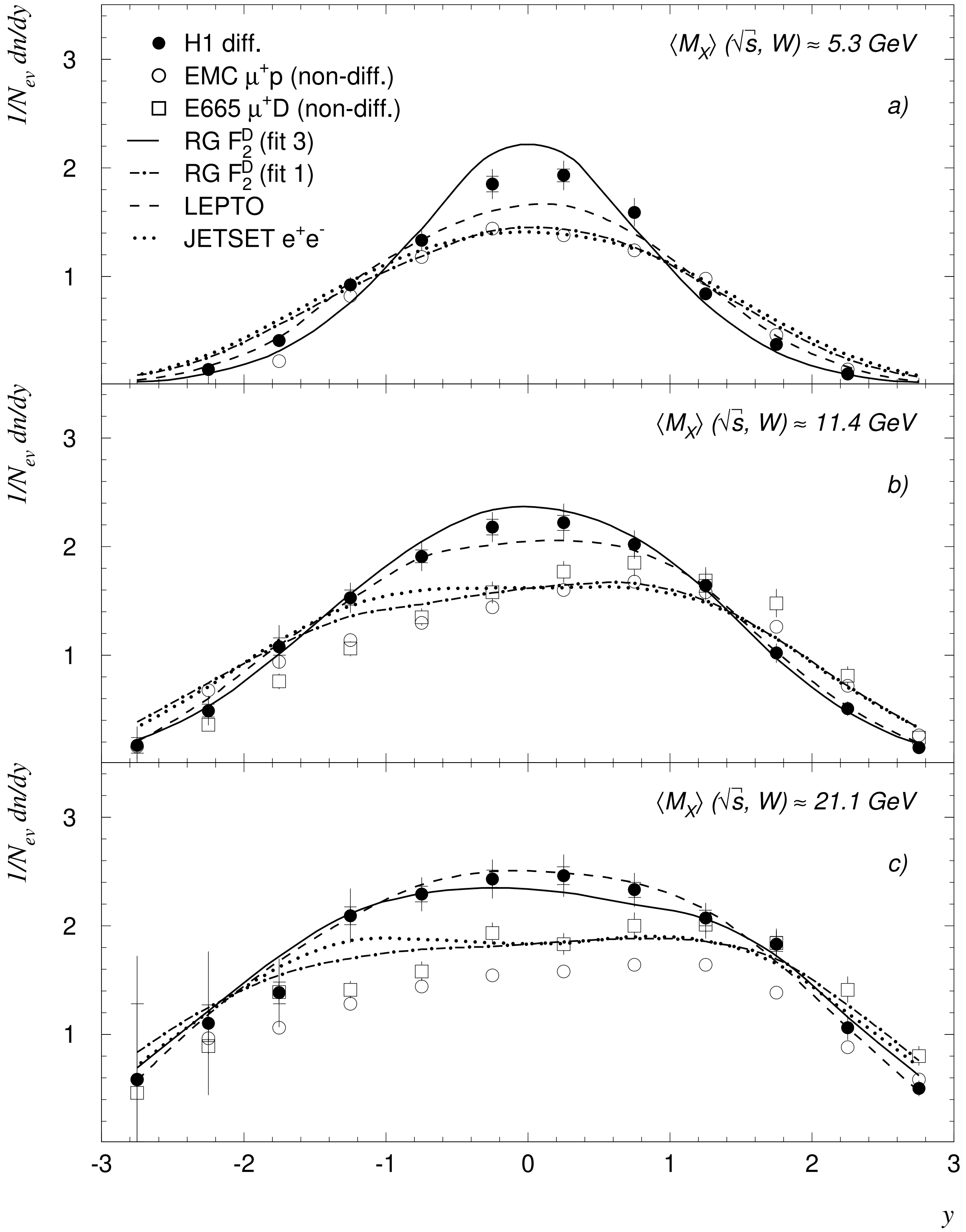

Figure 3: Charged particle rapidity spectra for three intervals in M_X (H1), at $W = \langle M_X \rangle$ (μN) and at $\sqrt{s} = \langle M_X \rangle$ (JETSET e^+e^-). The $\langle W \rangle$ values for EMC and E665 differ slightly from the ones indicated for H1 and are equal to 5.2, 11 and 19 GeV and 11.4 and 23.6 GeV, respectively. Also shown are predictions of several Monte Carlo models (see text).

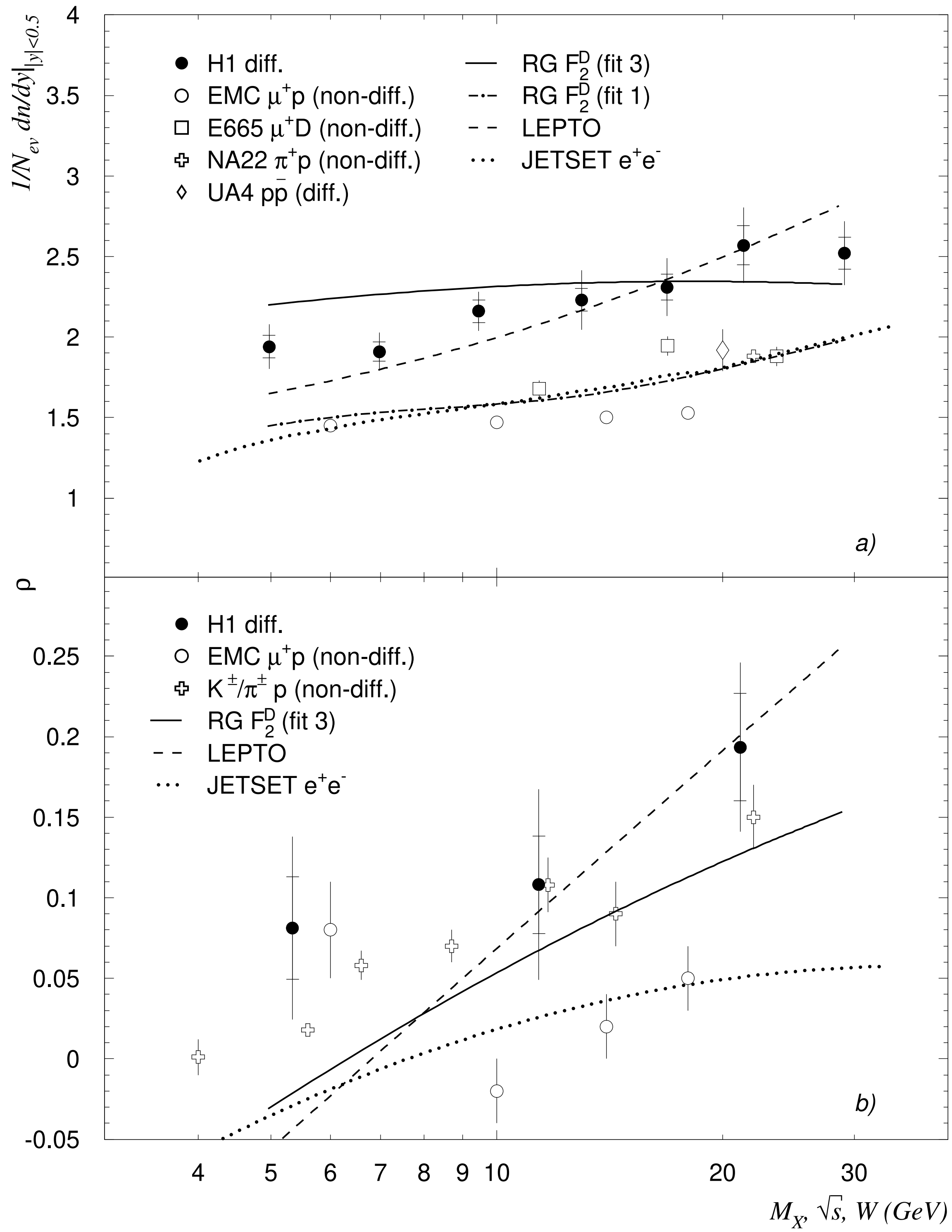

Figure 4: **(a)** Central region charged particle density ($-0.5 < y < 0.5$); **(b)** The parameter ρ (H1) and b (others), which reflects the correlation between the number of particles in the forward and backward hemispheres, as a function of M_X (H1), $W = \langle M_X \rangle$ (μp), M_X (hadron diffraction), $\sqrt{s}$ (non-diffractive hadron-hadron), $\sqrt{s}$ (JETSET e^+e^-). Also shown are predictions of several DIS Monte Carlo models (see text).